

Article

# Crystal Structure of Kristiansenite from Szklarska Poręba, Southwestern Poland

R. James Evans <sup>1</sup>, Bożena Gołębiowska <sup>2</sup>, Lee A. Groat <sup>1</sup> and Adam Pieczka <sup>2,\*</sup>

<sup>1</sup> Department of Earth, Ocean and Atmospheric Sciences, University of British Columbia, 6339 Stores Road, Vancouver, BC V6T 1Z4, Canada; rjamesevans@gmail.com (R.J.E.); groat@mail.ubc.ca (L.A.G.)

<sup>2</sup> Department of Mineralogy, Petrography and Geochemistry, AGH University of Science and Technology, Mickiewicza 30, 30-059 Kraków, Poland; goleb@agh.edu.pl

\* Correspondence: pieczka@agh.edu.pl; Tel.: +48-12-633-43-30

Received: 28 October 2018; Accepted: 7 December 2018; Published: 11 December 2018



**Abstract:** Kristiansenite, ideally  $\text{Ca}_2\text{ScSn}(\text{Si}_2\text{O}_7)(\text{Si}_2\text{O}_6\text{OH})$ , a rare late-stage hydrothermal Sc-bearing sorosilicate mineral, was found in a gadolinite-fergusonite-type pegmatite of the MI-REE subclass related to the Karkonosze granite, exposed in a quarry at Szklarska Poręba, Lower Silesia, Poland. Kristiansenite occurs in an association with andradite, epidote, allanite-(Ce), titanite, fersmite, scheelite, Sc-bearing columbite-(Fe), a  $\text{YNbO}_4$  mineral as fergusonite-(Y) or fergusonite-(Y)-beta, silesiaite and wolframite. Single-crystal study of the mineral ( $R_1$  of 4.96%), with composition  $\text{Ca}_{2.00}(\text{Sn}_{0.97}\text{Sc}_{0.69}\text{Fe}^{3+}_{0.17}\text{Mn}_{0.05}\text{Ti}_{0.04}\text{Zr}_{0.03}\text{Nb}_{0.02}\text{Al}_{0.02}\text{Ta}_{0.01})_{\Sigma 2}(\text{Si}_2\text{O}_7)[(\text{Si}_{1.98}\text{Al}_{0.02})_{\Sigma 2}\text{O}_{6.03}(\text{OH})_{0.97}]$ , corroborates its triclinic structure with space group-symmetry  $C1$ ,  $Z = 2$ , and unit-cell parameters  $a = 10.0304(5)$ ,  $b = 8.4056(4)$ ,  $c = 13.3228(6)$  Å,  $\alpha = 90.001(3)$ ,  $\beta = 109.105(3)$ ,  $\gamma = 89.997(3)^\circ$  and  $V = 1061.40(9)$  Å<sup>3</sup>. In the structure of the mineral, the Ca and Si sites are dominantly occupied with Ca and Si, whereas the  $M1$ – $M4$  sites are disordered. The  $M3$  and  $M4$  sites are occupied dominantly by Sn and subordinately Sc, whereas the  $M1$  and  $M2$  sites are occupied dominantly by Sc and subordinately by remaining occupants, including Sn.

**Keywords:** kristiansenite; chemical composition; structure refinement; pegmatite; Szklarska Poręba; Poland

## 1. Introduction

Kristiansenite, ideally  $\text{Ca}_2\text{ScSn}(\text{Si}_2\text{O}_7)(\text{Si}_2\text{O}_6\text{OH})$ , is a rare Sc-bearing sorosilicate mineral of Nb-Y-F (NYF) type pegmatites first found in a pegmatite of the amazonite–cleavelandite type at Heftetjern, Tørdal, Telemark, Norway [1]. Next the mineral was found in pegmatites from the Italian Alps in the Baveno region (Locatelli quarry and Seula mine [2,3]), and in a granitic pegmatite from Cadalso de los Vidrios near Madrid, Spain [4]. Recently, Vývavsky et al. [5] noted the presence of kristiansenite in the intragranitic NYF-affiliated pegmatite Kožichovice II, Třebíč pluton, Czech Republic, as a product of late Ca metasomatism of the primary thortveitite,  $\text{Sc}_2\text{Si}_2\text{O}_7$ . The crystal structure of type kristiansenite from Norway (triclinic; space group-symmetry  $C1$ ,  $Z = 2$ ) was solved by Ferraris et al. [6].

In this paper, we discuss the crystal chemistry and structure of kristiansenite found in a NYF-affiliated pegmatite in the Szklarska Poręba Huta quarry in Lower Silesia, southwestern Poland, related to post-magmatic stages in the Karkonosze granite intrusion.

## 2. Geological Setting

The Karkonosze granite is the largest Variscan pluton in the Western Sudetes at the northeastern margin of the Bohemian Massif. In Poland, it extends among Jelenia Góra and Janowice Wielkie on

the northeast, Kowary and Śnieżka Mt. to the south, and spreads to the west up to Liberec in the Czech Republic (Figure 1). The main rocks of the massif are porphyritic to equigranular biotite-bearing granite associated with a small volume of two-mica granite and subordinate granophyric granite [7,8], locally with lamprophyre and aplite dykes. The pluton is considered as a syn-collisional magmatic arc intrusion on the active margin of a continental platform neighboring oceanic crust, crystallized from relatively reduced, K-rich, calc-alkaline, highly evolved, mostly peraluminous I-type to transitional I-S type magmas ~320–310 Ma [9–16].

Pegmatites are particularly abundant in the porphyritic Karkonosze granite, and less frequent in the metamorphic cover of the granite massif. Most of them are barren, but there are also widespread weakly to moderately fractionated rare element-bearing pegmatites of NYF affiliation [17]. Intragranitic pegmatites usually form zoned pods, lenses and, more rarely, dikes of length ranging from centimetres to several decimetres, exceptionally several metres, whereas the pegmatites intruding the metamorphic cover are discordant massive dikes and lenticular bodies. In the classification of Černý and Ercit [18], the Karkonosze pegmatites correspond mainly to (i) podiform and lenticular gadolinite-fergusonite type intragranitic pegmatites of the miarolitic—rare-earth-elements (MI-REE) subclass; (ii) barren, schorl-bearing thin dikes, cutting discordantly the metamorphic envelope closest the granite.



**Figure 1.** Geological sketch of the Polish part of the Karkonosze granite massif with its metamorphic envelope. Abbreviations: ISB—Intra-Sudetic Basin. Symbols: star—the quarry at Szklarska Poręba, black lines—faults.

### 3. Occurrence

The Szklarska Poręba Huta quarry, located within a town Szklarska Poręba near Jelenia Góra, is currently the only place in the Polish part of the massif where granite is exploited, mainly as dimension stone. Small bodies of granitic NYF-type pegmatite, forming lenses and nests up to several tens of centimeters across, are relatively frequent within the coarsely crystalline variety of the porphyritic to equigranular granite; smaller nests up to only a few centimeters across and very often with a small cavity in the centre, are frequent in the granophyre granite.

Pegmatite mineralization in the porphyritic to equigranular granite, small primary cavities within granophyre granite, and in quartz veinlets cutting the granite, all with superimposed W-Sn-Mo-Bi and Th-U-REE ore assemblages, is represented by numerous REE-bearing phases, e.g., xenotime-(Y), monazite-(Ce), a  $\text{YNbO}_4$  mineral as fergusonite-(Y) or fergusonite-(Y)-beta, allanite-(Ce), yttrialite-(Y), gadolinite-(Y), gadolinite-(Ce) and hingganite-(Y); Nb-bearing phases, e.g., the mentioned  $\text{YNbO}_4$  mineral, columbite-(Fe) and fersmite; and Sc-bearing phases, e.g., thortveitite, scandium columbite-(Fe) and rare kristiansenite and its Fe-analogue, silesiaite, recently approved by the Commission on New Minerals, Nomenclature and Classification (CNMNC) of the International Mineralogical Association [19], and many other more common minerals [20–26]. Kristiansenite has been found

in small cavities of the equigranular granite in an assemblage composed of Ca-bearing minerals such as andradite grading to grossular garnet, epidote, allanite-(Ce), titanite and Sn-bearing titanite, fersmite and scheelite, Sc-bearing columbite-(Fe), fergusonite-(Y) or fergusonite-(Y)-beta, wolframite and marcasite. Locally, along with thortveitite, it forms numerous minute inclusions in scheelite.

#### 4. Materials and Methods

##### 4.1. Electron-Microprobe Analysis

Electron-microprobe analysis (EMPA) of kristiansenite was performed at the Inter-Institute Analytical Complex for Minerals and Synthetic Substances at the University of Warsaw, using a Cameca SX 100 electron microprobe operating in wavelength-dispersive mode under the following conditions: accelerating voltage of 15 kV, beam current of 20 nA, beam diameter of 2  $\mu\text{m}$ , peak count-time of 20 s, and background time of 10 s. Standards, diffracting crystals, analytical lines, and mean detection limits (in wt. %) were as follows: albite—Na (TAP,  $K\alpha$ , 0.02), diopside—Mg (TAP,  $K\alpha$ , 0.02), Si (TAP,  $K\alpha$ , 0.03) and Ca (PET,  $K\alpha$ , 0.04), orthoclase—Al (TAP,  $K\alpha$ , 0.03), rutile—Ti (PET,  $K\alpha$ , 0.09), rhodonite—Mn (LIF,  $K\alpha$ , 0.12), hematite—Fe (LIF,  $K\alpha$ , 0.12),  $\text{LiNbO}_3$ —Nb (PET,  $L\alpha$ , 0.10),  $\text{LiTaO}_3$ —Ta (TAP,  $M\alpha$ , 0.10), cassiterite—Sn (LPET,  $L\alpha$ , 0.07), zircon—Zr (LPET,  $L\alpha$ , 0.07), pure Sc—Sc (LPET,  $K\alpha$ , 0.02). The raw data were reduced with the PAP routine [27]. Atomic contents were normalized in relation to totals of eight cations and 14 oxygen atoms per formula unit (*apfu*), with the OH content calculated from electroneutrality of the formula, assuming all Fe as  $\text{Fe}^{3+}$ .

##### 4.2. Crystal Structure Refinement

Single-crystal X-ray diffraction measurements were made at C-HORSE (the Centre for Higher Order Structure Elucidation, in the Department of Chemistry at University of British Columbia) on a kristiansenite crystal  $45 \times 60 \times 40 \mu\text{m}$ , using a Bruker X8 APEX II diffractometer with graphite monochromated  $\text{MoK}\alpha$  radiation, at a crystal-to-detector distance of 40 mm. The data were collected at 100 K to a maximum  $2\theta$  value of  $60.2^\circ$ , in a series of  $\phi$  and  $\omega$  scans in  $0.50^\circ$  oscillations with 60 s exposures, integrated using the Bruker SAINT software package [28], and corrected for absorption effects using the multi-scan technique (SADABS; [29]), and for Lorentz and polarization effects. As the sample diffracted only weakly, a long collection time (48 h) was required to acquire enough reflections for a refinement. The collection was performed at 100 K to reduce noise from thermal vibrations. All refinements were performed using the SHELXTL crystallographic software package [30] of Bruker AXS. The weighting scheme was based on counting statistics. Neutral atom scattering factors were taken from Cromer and Waber [31]. Anomalous dispersion effects were included in  $F_{\text{calc}}$  [32]; the values for  $\Delta f'$  and  $\Delta f''$  were those of Creagh and McAuley [33]. The values for the mass attenuation coefficients are those of Creagh and Hubbell [34].

The structure was solved by direct methods [30] in the monoclinic space group  $C2/c$ , as indicated by experiment, using neutral atom scattering factors, and refined to an  $R_1$  index of 6.45% with anisotropic displacement parameters. However, in their original description of kristiansenite, Ferraris et al. [6] found that the crystals of kristiansenite typically show metric merohedral twinning. While the underlying structure including cation ordering is triclinic, the twin law belonging to the higher Laue group makes the structure appear monoclinic within experimental error. However, the presence of cation ordering at the octahedral *M* sites reveals the triclinic structure. The triclinic structure was derived from the monoclinic structure using online software at the Bilbao Crystallographic Server [35], with atomic positions in the triclinic structure based directly on equivalent positions in the monoclinic structure. The position of Ca1 was fixed arbitrarily as the origin. Following [6], the structure was refined to an  $R_1$  index of 4.96% in the unconventional triclinic space group setting  $C1$ .

## 5. Results

Compositional data from EMPA of the studied kristiansenite are presented in Table 1. Atomic contents for the averaged analysis (4 spots), give the following empirical formula of the mineral:  $\text{Ca}_{2.00}(\text{Sn}_{0.97}\text{Sc}_{0.69}\text{Fe}^{3+}_{0.17}\text{Mn}_{0.05}\text{Ti}_{0.04}\text{Zr}_{0.03}\text{Nb}_{0.02}\text{Al}_{0.02}\text{Ta}_{0.01})_{\Sigma 2}(\text{Si}_2\text{O}_7)[(\text{Si}_{1.98}\text{Al}_{0.02})_{\Sigma 2}\text{O}_{6.03}(\text{OH})_{0.97}]$ . Details of the data measurement and structure solution are listed in Table 2. Atomic coordinates, equivalent isotropic-displacement parameters, and occupancy for atomic sites in the kristiansenite are given in Table 3. Selected bond lengths and bond angles are collected in Table 4, and a bond-valence calculation is shown in Table 5. Anisotropic displacement parameters are presented in CIF file attached as Supplementary Materials.

**Table 1.** Average electron-microprobe analysis of kristiansenite from Szklarska Poręba ( $n = 4$ ).

Constituent	wt. %	apfu
Ta <sub>2</sub> O <sub>5</sub>	0.47	0.01
Nb <sub>2</sub> O <sub>5</sub>	0.49	0.02
SiO <sub>2</sub>	40.78	3.98
TiO <sub>2</sub>	0.50	0.04
ZrO <sub>2</sub>	0.56	0.03
SnO <sub>2</sub>	24.79	0.97
Al <sub>2</sub> O <sub>3</sub>	0.29	0.03
Sc <sub>2</sub> O <sub>3</sub>	8.16	0.69
Fe <sub>2</sub> O <sub>3</sub> *	2.34	0.17
MnO	0.64	0.05
CaO	19.11	2.00
H <sub>2</sub> O <sub>(calc.)</sub>	1.49	0.97
Total	99.61	

$n$ —number of analytical spots; Na and Mg were below detection; \*—calculated assuming all Fe as Fe<sup>3+</sup>.

**Table 2.** Data measurement and refinement information for kristiansenite.

Crystal Data	
Crystal size (mm)	0.045 × 0.060 × 0.040
Space group	C1
$a$ (Å)	10.0304(5)
$b$ (Å)	8.4056(4)
$c$ (Å)	13.3228(6)
$\alpha$	90.001(3)
$\beta$	109.105(3)
$\gamma$	89.997(3)
$V$ (Å <sup>3</sup> )	1061.40(9)
$Z$	2
Data Collection and Refinement	
Radiation	MoK $\alpha$
Monochromator	graphite
Temperature	100 K
Total $F_o$	29,210
Unique $F_o$	6213
$F_o > 4\sigma F_o$	4503
Range of $h, k, l$	$-14 \leq h \leq 14, -11 \leq k \leq 11, -18 \leq l \leq 18$
Max. $2\theta$ (°)	60.17
Inversion twin components	0.956:0.044

Table 2. Cont.

$R_{\text{int}}$	0.0936
L.s. parameters	339
$R_1$ for $F_o > 4\sigma F_o$	0.0496
$R_1$ , all unique $F_o$	0.0836
$wR_2$	0.1141
a	0.0497
b	0.00
GooF	1.052

Note:  $w = 1/[\sigma^2(F_o^2) + (a \times P)^2 + b \times P]$ , where  $P = [\text{Max}(F_o^2, 0) + 2 \times F_c^2]/3$ .

**Table 3.** Atomic coordinates, equivalent isotropic displacement parameters, and occupancy for atomic sites in kristiansenite (the occupancy for anion sites are from bond valence analysis).

	x	y	z	$U_{\text{eq}}$	Occupancy
Ca1	0	0	0	0.0177(6)	Ca
Ca2	0.0010(4)	0.7003(4)	−0.4984(3)	0.0171(6)	Ca
Ca3	0.2017(4)	−0.0030(4)	−0.2699(3)	0.0177(7)	Ca
Ca4	0.2019(2)	0.7035(2)	−0.7699(2)	0.0166(6)	Ca
M1	−0.2522(4)	0.0879(4)	−0.2458(3)	0.0084(6)	0.214(5) Sn + 0.787(5) Sc
M2	−0.2530(3)	0.6135(4)	−0.7469(3)	0.0104(5)	0.339(5) Sn + 0.661(5) Sc
M3	0.4605(3)	0.0856(3)	−0.0262(3)	0.0073(4)	0.785(6) Sn + 0.215(6) Sc
M4	0.4607(3)	0.6146(3)	−0.5255(3)	0.0089(4)	0.798(6) Sn + 0.202(6) Sc
Si1	−0.2317(5)	0.2728(5)	−0.0195(4)	0.0089(7)	Si
Si2	−0.2319(5)	0.4280(5)	−0.5194(4)	0.0093(7)	Si
Si3	0.4362(5)	0.2748(5)	−0.2527(4)	0.0086(8)	Si
Si4	0.4359(5)	0.4260(5)	−0.7531(4)	0.0088(7)	Si
Si5	−0.0276(5)	0.3829(5)	−0.8161(4)	0.0086(7)	Si
Si6	−0.0276(5)	0.3182(5)	−0.3164(4)	0.0093(7)	Si
Si7	0.2286(5)	0.3824(5)	−0.4567(4)	0.0094(7)	Si
Si8	0.2281(5)	0.3185(5)	0.0433(4)	0.0092(7)	Si
O1	0.575(1)	0.255(1)	−0.2877(9)	0.015(2) *	O
O2	0.5808(10)	0.446(1)	−0.7846(8)	0.009(2) *	O
O3	−0.371(1)	0.256(1)	0.0136(9)	0.015(2)	O
O4	−0.3756(10)	0.444(1)	−0.4871(8)	0.007(2)	O
O5	−0.071(1)	−0.0512(10)	−0.2004(8)	0.012(2)	O
O6	−0.0688(10)	0.7518(10)	−0.7013(7)	0.010(2) *	O
O7	0.279(1)	−0.053(1)	−0.0687(8)	0.014(2)	O
O8	0.276(1)	0.753(1)	−0.5689(8)	0.013(2)	O
O9	−0.211(1)	0.128(1)	−0.0914(8)	0.012(2)	O
O10	−0.211(1)	0.573(1)	−0.5911(8)	0.010(2) *	O
O11	0.413(1)	0.128(1)	−0.1813(8)	0.011(2)	O
O12	0.414(1)	0.573(1)	−0.6817(8)	0.010(2) *	O
O13	−0.0941(10)	0.252(1)	0.0908(7)	0.012(2)	O
O14	−0.0940(9)	0.4488(10)	−0.4087(7)	0.010(2) *	O
O15	0.2999(9)	0.251(1)	−0.3601(7)	0.014(2)	O
O16	0.3004(10)	0.450(1)	−0.8614(8)	0.013(2) *	O
O17	−0.139(1)	0.284(1)	−0.2584(8)	0.009(2) *	O
O18	−0.147(1)	0.418(1)	−0.7629(8)	0.009(2) *	O
O19	0.344(1)	0.284(1)	−0.0150(8)	0.012(2)	O
O20	0.353(1)	0.416(1)	−0.5079(8)	0.014(2)	O
O21	−0.3117(10)	0.0388(10)	−0.4038(7)	0.010(2)	O
O22	−0.3117(10)	0.659(1)	0.0966(7)	0.012(2)	O
O23	0.5155(10)	0.039(1)	−0.8674(8)	0.012(2) *	O
O24	0.516(1)	0.659(1)	−0.3675(8)	0.013(2)	O
O25	−0.3834(10)	−0.107(1)	−0.2289(8)	0.015(2)	O
O26	−0.3852(9)	0.807(1)	−0.7313(7)	0.012(2)	O
O27	0.5868(10)	−0.0979(10)	−0.0419(8)	0.012(2) *	O
O28	0.5908(10)	0.7993(10)	−0.5393(7)	0.007(2) *	O

Note: \*  $U_{\text{iso}}$ .

**Table 4.** Bond lengths (Å) and bond angles (°) for kristiansenite.

Ca1-O22	2.327(9)	Ca2-O20	2.319(10)
Ca1-O9	2.328(10)	Ca2-O21	2.328(9)
Ca1-O19	2.362(10)	Ca2-O10	2.344(9)
Ca1-O3	2.398(10)	Ca2-O4	2.375(9)
Ca1-O5	2.564(10)	Ca2-O6	2.599(9)
Ca1-O2	2.753(10)	Ca2-O1	2.699(11)
Ca1-O13	2.757(8)	Ca2-O14	2.747(8)
<Ca1-O>	2.498	<Ca2-O>	2.487
O2-Ca1-O3	79.3(3)	O1-Ca2-O4	80.0(3)
O2-Ca1-O13	72.3(3)	O1-Ca2-O14	72.3(3)
O2-Ca1-O19	85.6(3)	O1-Ca2-O20	82.7(3)
O2-Ca1-O22	66.9(3)	O1-Ca2-O21	68.8(3)
O3-Ca1-O5	83.9(3)	O4-Ca2-O6	83.1(3)
O3-Ca1-O19	71.0(3)	O4-Ca2-O20	68.8(3)
O3-Ca1-O22	97.4(3)	O4-Ca2-O21	99.1(3)
O5-Ca1-O9	68.7(3)	O6-Ca2-O10	68.9(3)
O5-Ca1-O19	80.4(3)	O6-Ca2-O20	82.3(3)
O5-Ca1-O22	124.8(3)	O6-Ca2-O21	123.7(3)
O9-Ca1-O13	59.5(3)	O10-Ca2-O14	59.5(3)
O9-Ca1-O19	81.3(4)	O10-Ca2-O20	82.7(3)
O9-Ca1-O22	117.3(3)	O10-Ca2-O21	117.0(3)
O13-Ca1-O19	108.5(3)	O14-Ca2-O20	108.5(3)
O13-Ca1-O22	69.4(3)	O14-Ca2-O21	69.5(3)
Ca3-O24	2.325(10)	Ca4-O18	2.340(9)
Ca3-O11	2.335(10)	Ca4-O12	2.342(10)
Ca3-O1	2.367(10)	Ca4-O23	2.347(9)
Ca3-O17	2.370(9)	Ca4-O2	2.348(9)
Ca3-O7	2.568(10)	Ca4-O8	2.569(10)
Ca3-O4	2.775(10)	Ca4-O3	2.772(12)
Ca3-O15	2.785(9)	Ca4-O16	2.794(9)
<Ca3-O>	2.504	<Ca4-O>	2.501
O4-Ca3-O1	78.6(3)	O3-Ca4-O2	79.8(3)
O4-Ca3-O15	72.0(3)	O3-Ca4-O16	71.2(3)
O4-Ca3-O17	84.4(3)	O3-Ca4-O18	82.3(3)
O4-Ca3-O24	67.1(3)	O3-Ca4-O23	68.2(3)
O1-Ca3-O7	86.2(3)	O2-Ca4-O8	84.9(3)
O1-Ca3-O17	71.7(3)	O2-Ca4-O18	69.3(3)
O1-Ca3-O24	98.0(4)	O2-Ca4-O23	99.8(3)
O7-Ca3-O11	68.4(3)	O8-Ca4-O12	69.3(3)
O7-Ca3-O17	80.7(3)	O8-Ca4-O18	82.5(3)
O7-Ca3-O24	126.4(3)	O8-Ca4-O23	125.4(3)
O11-Ca3-O15	57.8(3)	O12-Ca4-O16	57.8(3)
O11-Ca3-O17	81.0(3)	O12-Ca4-O18	82.4(3)
O11-Ca3-O24	115.8(3)	O12-Ca4-O23	115.5(3)
O15-Ca3-O17	106.5(3)	O16-Ca4-O18	106.7(3)
O15-Ca3-O24	69.0(3)	O16-Ca4-O23	68.9(3)
M1-O9	1.989(9)	M2-O22	2.008(8)
M1-O17	2.035(9)	M2-O18	2.009(9)
M1-O21	2.037(9)	M2-O10	2.011(9)
M1-O5	2.078(9)	M2-O6	2.099(9)
M1-O25	2.159(10)	M2-O2	2.113(9)
M1-O1	2.163(10)	M2-O26	2.153(9)
<M1-O>	2.077	<M2-O>	2.065

Table 4. Cont.

O9-M1-O17	90.7(4)	O22-M2-O18	91.8(4)
O9-M1-O5	85.8(4)	O22-M2-O6	97.2(3)
O9-M1-O25	87.1(4)	O22-M2-O2	86.5(3)
O9-M1-O1	92.0(4)	O22-M2-O26	88.6(3)
O17-M1-O21	93.6(4)	O18-M2-O10	92.0(4)
O17-M1-O5	91.2(4)	O18-M2-O6	92.1(4)
O17-M1-O1	82.7(4)	O18-M2-O2	80.5(4)
O21-M1-O5	96.8(4)	O10-M2-O6	86.1(4)
O21-M1-O25	88.4(4)	O10-M2-O2	90.7(4)
O21-M1-O1	85.8(4)	O10-M2-O26	87.4(3)
O5-M1-O25	92.9(4)	O6-M2-O26	93.7(3)
O25-M1-O1	93.1(4)	O2-M2-O26	93.7(3)
M3-O11	1.991(9)	M4-O12	2.010(9)
M3-O23	2.044(9)	M4-O24	2.024(9)
M3-O27	2.050(9)	M4-O20	2.042(9)
M3-O19	2.067(9)	M4-O28	2.074(8)
M3-O7	2.073(9)	M4-O8	2.102(9)
M3-O3	2.145(9)	M4-O4	2.110(9)
<M3-O>	2.061	<M4-O>	2.06
O11-M3-O27	88.5(4)	O12-M4-O20	91.6(4)
O11-M3-O19	89.0(4)	O12-M4-O28	88.6(4)
O11-M3-O7	85.6(4)	O12-M4-O8	85.8(4)
O11-M3-O3	92.2(4)	O12-M4-O4	91.8(4)
O23-M3-O27	89.8(3)	O24-M4-O20	90.2(4)
O23-M3-O19	92.7(4)	O24-M4-O28	89.4(4)
O23-M3-O7	95.2(4)	O24-M4-O8	95.9(4)
O23-M3-O3	87.2(4)	O24-M4-O4	86.8(4)
O27-M3-O7	93.8(4)	O20-M4-O8	92.0(4)
O27-M3-O3	93.7(4)	O20-M4-O4	79.4(4)
O19-M3-O7	90.3(4)	O28-M4-O8	94.7(3)
O19-M3-O3	82.0(4)	O28-M4-O4	93.9(3)
Si1-O3	1.603(10)	Si2-O10	1.600(10)
Si1-O9	1.606(10)	Si2-O8	1.624(10)
Si1-O7	1.627(10)	Si2-O4	1.640(9)
Si1-O13	1.663(9)	Si2-O14	1.667(9)
<Si1-O>	1.625	<Si2-O>	1.633
O3-Si1-O9	113.1(5)	O4-Si2-O14	107.8(5)
O3-Si1-O7	111.7(6)	O8-Si2-O4	110.3(5)
O3-Si1-O13	107.2(5)	O8-Si2-O14	108.5(5)
O9-Si1-O7	113.8(5)	O10-Si2-O8	114.4(5)
O9-Si1-O13	102.5(5)	O10-Si2-O4	112.7(5)
O7-Si1-O13	107.7(5)	O10-Si2-O14	102.5(5)
Si3-O1	1.612(11)	Si4-O12	1.617(10)
Si3-O11	1.626(10)	Si4-O6	1.624(9)
Si3-O5	1.634(9)	Si4-O16	1.639(10)
Si3-O15	1.636(9)	Si4-O2	1.649(10)
<Si3-O>	1.627	<Si4-O>	1.632
O1-Si3-O11	113.4(5)	O6-Si4-O16	110.5(5)
O1-Si3-O5	112.1(5)	O6-Si4-O2	110.5(5)
O1-Si3-O15	106.7(5)	O12-Si4-O6	114.5(5)
O5-Si3-O15	109.9(5)	O12-Si4-O16	101.1(5)
O11-Si3-O5	113.4(5)	O12-Si4-O2	111.7(5)
O11-Si3-O15	100.4(5)	O16-Si4-O2	108.0(5)
Si5-O23	1.598(9)	Si6-O17	1.586(10)
Si5-O18	1.602(10)	Si6-O14	1.623(9)
Si5-O13	1.626(9)	Si6-O24	1.631(10)
Si5-O26	1.633(9)	Si6-O25	1.655(10)
<Si5-O>	1.615	<Si6-O>	1.624

Table 4. Cont.

O13-Si5-O26	108.2(5)	O14-Si6-O24	109.9(5)
O18-Si5-O13	106.4(5)	O14-Si6-O25	108.8(5)
O18-Si5-O26	112.1(5)	O17-Si6-O14	108.4(5)
O23-Si5-O18	112.3(5)	O17-Si6-O24	112.7(5)
O23-Si5-O13	109.3(5)	O17-Si6-O25	108.5(5)
O23-Si5-O26	108.5(5)	O24-Si6-O25	108.4(5)
Si7-O21	1.602(9)	Si8-O19	1.625(10)
Si7-O28	1.619(9)	Si8-O22	1.632(9)
Si7-O20	1.630(10)	Si8-O27	1.655(10)
Si7-O15	1.666(9)	Si8-O16	1.659(9)
<Si7-O>	1.629	<Si8-O>	1.643
O20-Si7-O15	104.0(5)	O19-Si8-O22	112.2(5)
O21-Si7-O28	111.8(5)	O19-Si8-O27	109.6(5)
O21-Si7-O20	112.2(5)	O19-Si8-O16	106.5(5)
O21-Si7-O15	108.0(5)	O22-Si8-O27	111.8(5)
O28-Si7-O20	113.2(5)	O22-Si8-O16	108.7(5)
O28-Si7-O15	107.2(5)	O27-Si8-O16	107.8(5)

Table 5. Bond valences (calculated with parameters from Brese and O'Keefe, [36]).

Cations		Anions	
Ca1:Ca <sup>2+</sup>	1.85	O1:O <sup>2-</sup>	1.93
Ca2:Ca <sup>2+</sup>	1.90	O2:O <sup>2-</sup>	1.89
Ca3:Ca <sup>2+</sup>	1.84	O3:O <sup>2-</sup>	1.98
Ca4:Ca <sup>2+</sup>	1.86	O4:O <sup>2-</sup>	1.95
M1:Sn <sup>4+</sup>	3.83	O5:O <sup>2-</sup> , (OH) <sup>-</sup>	1.70
M1:Sc <sup>3+</sup>	2.58	O6:O <sup>2-</sup> , (OH) <sup>-</sup>	1.68
M1:Fe <sup>3+</sup>	3.29	O7:O <sup>2-</sup> , (OH) <sup>-</sup>	1.80
M2:Sn <sup>4+</sup>	3.94	O8:O <sup>2-</sup> , (OH) <sup>-</sup>	1.76
M2:Sc <sup>3+</sup>	2.65	O9:O <sup>2-</sup>	2.09
M2:Fe <sup>3+</sup>	3.39	O10:O <sup>2-</sup>	2.06
M3:Sn <sup>4+</sup>	3.96	O11:O <sup>2-</sup>	2.12
M3:Sc <sup>3+</sup>	2.67	O12:O <sup>2-</sup>	2.11
M3:Fe <sup>3+</sup>	3.40	O13:O <sup>2-</sup>	2.01
M4:Sn <sup>4+</sup>	3.96	O14:O <sup>2-</sup>	2.01
M4:Sc <sup>3+</sup>	2.67	O15:O <sup>2-</sup>	1.97
M4:Fe <sup>3+</sup>	3.41	O16:O <sup>2-</sup>	1.98
Si1:Si <sup>4+</sup>	4.00	O17:O <sup>2-</sup>	2.04
Si2:Si <sup>4+</sup>	3.92	O18:O <sup>2-</sup>	2.07
Si3:Si <sup>4+</sup>	3.97	O19:O <sup>2-</sup>	1.96
Si4:Si <sup>4+</sup>	3.91	O20:O <sup>2-</sup>	2.03
Si5:Si <sup>4+</sup>	4.10	O21:O <sup>2-</sup>	2.03
Si6:Si <sup>4+</sup>	4.01	O22:O <sup>2-</sup>	2.00
Si7:Si <sup>4+</sup>	3.95	O23:O <sup>2-</sup>	2.09
Si8:Si <sup>4+</sup>	3.81	O24:O <sup>2-</sup>	2.06
		O25:(OH) <sup>-</sup> , O <sup>2-</sup>	1.34
		O26:(OH) <sup>-</sup> , O <sup>2-</sup>	1.41
		O27:O <sup>2-</sup> , (OH) <sup>-</sup>	1.57
		O28:O <sup>2-</sup> , (OH) <sup>-</sup>	1.62

## 6. Discussion

Taking into account accuracies in the microprobe analysis, it can be assumed that the Ca sites, with a lack of Na, are completely occupied by Ca, and the Si sites are dominantly occupied by Si, with a small deficiency completed by subordinate Al. The occupancies are corroborated by the refined

electron densities and occupancies of the sites (Table 3), as well as average  $\langle \text{Ca-O} \rangle$  distances in the 7-fold-coordinated Ca1–Ca4 polyhedra (2.487–2.504 Å; Table 4), and Si1–Si8 tetrahedra (1.615–1.643 Å).

The four *M* sites of the kristiansenite cell have very diverse occupants, dominated by tetravalent (Sn, Ti, Zr)<sup>4+</sup> and trivalent cations (Sc, Fe, Al)<sup>3+</sup>, respectively; however, trace amounts of divalent (Mn<sup>2+</sup>) and pentavalent (Nb, Ta)<sup>5+</sup> cations are also present. This is similar to the composition of the type material [1], but the presence of Mn, Nb, and Ta are new. The total charge of the *M*-site occupants in the formula unit equals 6.99 valence units, and the calculated H<sup>+</sup>, bonded to oxygen atoms coordinating Si, is 0.97 *apfu*; both nearly equal to the ideal values in the general composition of the mineral. Substitutions at the octahedral *M* sites must, therefore, be mutually charge-balanced to a high degree. These substitutions involve the distribution of cations among the *M* sites and lead to the observed disordering of the divalent to pentavalent *M*-type cations among the M1–M4 sites. The refined total content of electrons at the *M* sites of the unit cell, 145.9 e<sup>−</sup>, agrees well with 145.1 e<sup>−</sup> calculated from the EMPA formula. The structure refinement separates the electrons among the M1–M4 sites in the following way: 27.2(4); 30.8(3); 43.8(4); 44.1(4) e<sup>−</sup>, respectively, which leads to the Sn–Sc site occupancies presented in Table 3.

However, the real population of the *M*-site occupants is much more diversified than the simple Sn–Sc system. To approximate the distribution of octahedral cations among the M1–M4 sites, the refined electron densities at the sites were recalculated proportional to the value of 145.1 e<sup>−</sup> from the empirical microprobe formula: 27.1; 30.6; 43.6 and 43.9 e<sup>−</sup>. Note that the differences between the measured and calculated electron densities are smaller than the respective 1σ ranges in the refinement. Since the M4 and M3 sites have very similar high electron densities, Sn is predicted to be one of their main occupants. The remaining occupants were tested from various combinations of octahedral cations with the best results achieved for the pair Sn–Sc. The M4- and M3-site occupancies were calculated as (Sn<sub>0.788</sub>Sc<sub>0.212</sub>) and (Sn<sub>0.778</sub>Sc<sub>0.224</sub>), respectively, corresponding to the recalculated electron densities and featuring very realistic calculated averaged cation radii close to ~0.702 Å. The remaining M2 and M1 cations are highly dominated by Sc<sup>3+</sup> (0.957 *apfu* as a result of  $Z \cdot \text{Sc}_{\text{total}} - M^4\text{Sc} - M^3\text{Sc}$ ). Due to the predominance of Sc, the occupancies of the sites were analyzed in the system Sc–(X), where (X) denotes a complex cation average of the rest of the Sn and traces of all other octahedral cations. For such a system, the M2 occupancy were evaluated at (X<sub>0.640</sub>Sc<sub>0.360</sub>) and the M1 occupancy at (X<sub>0.403</sub>Sc<sub>0.597</sub>), respectively, for which the calculated averaged cation radii are equal to ~0.703 Å and ~0.716 Å, respectively. Formally, the M2 site is dominated by trivalent Sc + Fe (0.57 *apfu*) with dominant Sc (0.36 *apfu*), and the M1 site is highly dominated by Sc (0.60 *apfu*), with only subordinate Fe and Sn (0.13 and 0.14 *apfu*, respectively). The arrangement of the calculated averaged M1–M4 radii vs. the refined mean bond lengths in the M1–M4 octahedra (Table 4) is represented by an equation  $\langle M_i\text{-O} \rangle = 1.025 \cdot \langle r_i \rangle + 1.343$  with a correlation coefficient  $R^2 = 0.986$  that is very close to the ideal relationship  $\langle M_i\text{-O} \rangle = \langle r_i \rangle + r\text{O}^{2-}$  (Figure 2). It corroborates that in the studied kristiansenite from Szklarska Poręba, the M1 and M2 sites are dominated with Sc, and the M3 and M4 sites dominated with Sn. The distribution of cations among the sites is highly disordered, with visible preference of Sn–Sc disorder at the M3 and M4 sites, and Sc–X disorder at the M2 and M1 sites.

The kristiansenite unit cell contains two hydrogen atoms on average, shared among the O5–O8 and O25–O28 oxygens, but OH<sup>−</sup> only prevails over O<sup>2−</sup> at two sites, O25 bonded with M1 and O26 bonded with M2. The O25–O27 and O26–O28 distances, 2.604 and 2.641 Å respectively, imply the presence of two hydrogen bonds with the O25 and O26 donor oxygens (*b.v.* = −1.34 and −1.41; Table 5), and the O27 and O28 acceptor oxygens (*b.v.* = −1.57 and −1.62). The equivalent distances in the structure of type kristiansenite are 2.627 and 2.646 Å [5]. The presence of hydroxyl anions around the M1 and M2 sites dominated by M<sup>3+</sup> cations suggests a simple substitution  $M^{3+}\text{OH}(M^{4+}\text{O}^{2-})_{-1}$ . This also explains the subordinate presence of OH<sup>−</sup> at the O7–O8 sites coordinated around the M3 and M4 sites dominated by M<sup>4+</sup> cations, because subordinate amounts of M<sup>3+</sup>-type cations are present at the sites only due to the M<sup>3+</sup>–M<sup>4+</sup> disorder.

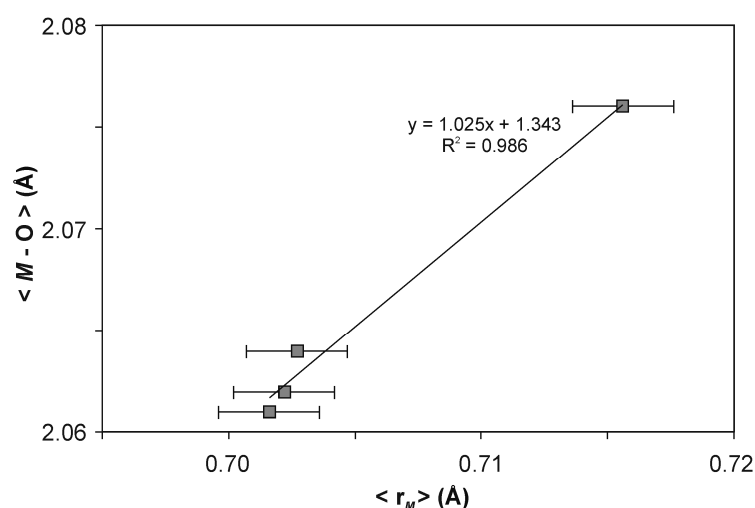


**Figure 2.** Variation of the  $M$  cation radius in octahedral coordination  $\langle r_M \rangle$  evaluated from the site scattering with the refined  $\langle M-O \rangle$  distances.

## 7. Conclusions

The gadolinite-fergusonite-type pegmatite of the MI-REE subclass related to the Karkonosze granite exposed in the Szklarska Poręba Huta granite quarry in Lower Silesia, Poland, is one of few known occurrences of kristiansenite,  $\text{Ca}_2\text{ScSn}(\text{Si}_2\text{O}_7)(\text{Si}_2\text{O}_6\text{OH})$ , a rare sorosilicate mineral. The mineral is associated with andradite, grossular, epidote, allanite-(Ce), titanite and Sn-bearing titanite, fersmite, scheelite, Sc-bearing columbite-(Fe), a  $\text{YNbO}_4$  mineral as fergusonite-(Y) or fergusonite-(Y)-beta, wolframites and marcasite, and represent a late-stage hydrothermal phase. The studied kristiansenite features a triclinic structure with space group-symmetry  $C1$ , and unit-cell parameters  $a = 10.0304(5)$ ,  $b = 8.4056(4)$ ,  $c = 13.3228(6)$  Å,  $\alpha = 90.001(3)$ ,  $\beta = 109.105(3)$ ,  $\gamma = 89.997(3)^\circ$  and  $V = 1061.40(9)$  Å<sup>3</sup> as collected at room temperature, very close to the cell of type kristiansenite [1,6]. Its unit cell can also be interpreted as monoclinic within the range of accuracy of the parameters, however, the presence of cation ordering at the octahedral  $M$  sites reveals its true triclinic structure. The Ca and Si sites in the structure of the kristiansenite are completely occupied by these elements, whereas the  $M1$ – $M4$  sites have very diversified occupants with the dominant tetravalent (Sn, Ti, Zr)<sup>4+</sup> and trivalent cations (Sc, Fe, Al)<sup>3+</sup>, and trace amounts of divalent (Mn<sup>2+</sup>) and pentavalent (Nb, Ta)<sup>5+</sup> cations, all disordered among the sites. The  $M4$  and  $M3$  sites are dominantly occupied by Sn and subordinately by Sc due to Sn–Sc disorder typical for the mineral. The  $M2$  and  $M1$  sites are filled dominantly by Sc and comprise all other divalent to pentavalent cations along with subordinate Sn due to the disorder among Sc and all other  $M$ -type occupants, including the rest Sn. Two hydrogen atoms are dominantly bonded with two oxygens coordinated around the  $M1$  and  $M2$  sites dominantly occupied by trivalent cations, suggesting  $M^{3+}\text{OH}(M^{4+}\text{O}^{2-})_{-1}$  substitution that controls the  $M$ -sites occupants and their lattice setting. Therefore, due to Sn–Sc disorder, a subordinate OH amount is also bonded to the  $M3$  and  $M4$  occupants. Hydroxyls coordinated around the  $M1$  and  $M2$  form hydrogen bonds with oxygens coordinated around  $M3$  and  $M4$  sites.

**Supplementary Materials:** The following are available online at <http://www.mdpi.com/2075-163X/8/12/584/s1>, CIF file for kristiansenite from Szklarska Poręba (Poland).

**Author Contributions:** A.P. and B.G. collected the kristiansenite sample, performed its E.M.P. analysis, made compositional calculations and prepared the figures, R.J.E. and L.A.G. made structural studies of the extracted crystal and described structure of the mineral; R.J.E. and A.P. wrote the manuscript.

**Funding:** This research was funded by the AGH UST grant no. 11.11.140.158 to A.P. and B.G.

**Conflicts of Interest:** The authors declare no conflict of interest. The funders had no role in the design of the study; in the collection, analyses, or interpretation of data; in the writing of the manuscript, and in the decision to publish the results.

## References

1. Raade, G.; Ferraris, G.; Gula, A.; Ivaldi, G.; Bernhard, F. Kristiansenite, a new calcium–scandium–tin sorosilicate from granite pegmatite in Tørdal, Telemark, Norway. *Miner. Petrol.* **2002**, *75*, 89–99. [[CrossRef](#)]
2. Guastoni, A.; Pezzotta, F. Kristiansenite a Baveno, secondo ritrovamento mondiale della specie. *Riv. Mineral. Ital.* **2004**, *4*, 247–251.
3. Nestola, F.; Guastoni, A.; Camara, F.; Secco, L.; Dal Negro, A.; Pedron, D.; Beran, A. Aluminocerite-(Ce): A new species from Baveno, Italy: Description and crystal-structure determination. *Am. Mineral.* **2009**, *94*, 487–493. [[CrossRef](#)]
4. Prado-Herrero, P.; Garcia-Guinea, J.; Crespo-Feo, E.; Correcher, V.; Menor, C. First find of Kristiansenite in Spain: Comparison with the type specimen by non-descriptive techniques. *Estudios Geológicos* **2009**, *19*, 135–139.
5. Výravský, J.; Škoda, R.; Novák, M. Kristiansenite, thortveitite and ScNbO<sub>4</sub>: Products of Ca-metasomatism of Sc-enriched columbite-(Mn) from NYF pegmatite Kožichovice II, Czech Republic. In Proceedings of the PEG2017 8th International Symposium on Granitic Pegmatites, Kristiansand, Norway, 13–15 June 2017; Müller, A., Rosing-Schow, N., Eds.; Norwegian Geological Society: Trondheim, Norway, 2017; Volume 2, pp. 169–172.
6. Ferraris, G.; Gula, A.; Ivaldi, G.; Nespolo, M.; Raade, G. Crystal structure of kristiansenite: A case of class IIB twinning by metric merohedry. *Z. Kristallogr.* **2001**, *216*, 442–448. [[CrossRef](#)]
7. Berg, G. Der Granit des Riesengebirges und seine Ganggesteine (Petrographische Studien). *Abh. Preuss. Geol. Land.* **1923**, *94*.
8. Borkowska, M. Petrography of Karkonosze granite. *Geol. Sudet.* **1966**, *2*, 7–119.
9. Duthou, J.-L.; Couturie, J.P.; Mierzejewski, M.P.; Pin, C. Age determination of the Karkonosze granite using the Rb-Sr isochrone whole-rock method. *Prz. Geol.* **1991**, *36*, 75–79. (In Polish)
10. Oberc-Dziedzic, T.; Żelaźniewicz, A.; Cwojdzinski, S. Granitoids of the Odra fault zone: Late to post-orogenic Variscan intrusions in the Saxothuringian zone, SW Poland. *Geol. Sudetica* **1999**, *32*, 55–71.
11. Mazur, S.; Aleksandrowski, P.; Turniak, K.; Awdankiewicz, M. Geology, tectonic evolution and Late Palaeozoic magmatism of Sudetes—An overview. *Granitoids Poland. AM Monogr.* **2007**, *1*, 59–87.
12. Mikulski, S.Z. Metal ore potential of the parent magma of granite—The Karkonosze massif example. *Granitoids Poland. AM Monogr.* **2007**, *1*, 123–145.
13. Słaby, E.; Martin, H. Mafic and felsic magma interaction in granites: The Hercynian Karkonosze pluton (Sudetes, Bohemian Massif). *J. Petrol.* **2008**, *49*, 353–391. [[CrossRef](#)]
14. Kryza, R.; Pin, C.; Oberc-Dziedzic, T.; Crowley, Q.G.; Larionov, A. Deciphering the geochronology of a large granitoid pluton (Karkonosze Granite, SW Poland): An assessment of U-Pb zircon SIMS and Rb-Sr whole-rock dates relative to U-Pb zircon CA-ID-TIMS. *Int. Geol. Rev.* **2014**, *56*, 756–782. [[CrossRef](#)]
15. Kryza, R.; Schaltegger, U.; Oberc-Dziedzic, T.; Pin, C.; Ovtcharova, M. Geochronology of a composite granitoid pluton: A high-precision ID-TIMS U-Pb zircon study of the Variscan Karkonosze Granite (SW Poland). *Int. J. Earth Sci.* **2014**, *103*, 683–696. [[CrossRef](#)]
16. Kusiak, M.A.; Williams, I.S.; Dunkley, D.J.; Konečný, P.; Słaby, E.; Martin, H. Monazite to the rescue: U-Th-Pb dating of the intrusive history of the composite Karkonosze pluton, Bohemian Massif. *Chem. Geol.* **2014**, *364*, 76–92. [[CrossRef](#)]
17. Pieczka, A.; Szuszkiewicz, A.; Szeleg, E.; Janeczek, J.; Nejbert, K. Granitic pegmatites of the Polish part of the Sudetes (NE Bohemian massif, SW Poland). In Proceedings of the PEG2015 7th International Symposium on Granitic Pegmatites, Książ, Poland, 17–19 June 2015; Gadas, P., Novák, M., Szuszkiewicz, A., Cempírek, J., Eds.; Tigris: Zlín, Czech Republic, 2015.
18. Černý, P.; Ercit, T.S. The classification of granitic pegmatites revisited. *Can. Mineral.* **2005**, *43*, 2005–2026. [[CrossRef](#)]
19. Pieczka, A.; Ma, C.; Rossman, G.R.; Evans, R.J.; Groat, L.A.; Gołębiewska, B. Silesiaite, IMA 2017-064. CNMNC Newsletter No. 40, December 2017, page 1578. *Mineral. Mag.* **2017**, *81*, 1577–1581. [[CrossRef](#)]
20. Karwowski, Ł.; Olszyński, W.; Kozłowski, A. Wolframite mineralization from the vicinity of Szklarska Poręba Huta. *Prz. Geol.* **1973**, *21*, 633–637. (In Polish)
21. Kozłowski, A.; Karwowski, Ł.; Olszyński, W. Tungsten-tin-molybdenum mineralization in the Karkonosze massif. *Acta Geol. Pol.* **1975**, *25*, 415–430.

22. Olszyński, W.; Kozłowski, A.; Karwowski, Ł. Bismuth minerals from the Karkonosze massif. *Acta Geol. Pol.* **1976**, *26*, 443–449.
23. Pieczka, A.; Gołębiowska, B. Pegmatites of the Szklarska Poręba Huta granite quarry: Preliminary data on REE mineralization. *Mineral. Spec. Pap.* **2002**, *20*, 175–177.
24. Pieczka, A.; Gołębiowska, B.; Ilnicki, S.; Dzierżanowski, P.; Jeżak, L. Gadolinite group minerals from Szklarska Poręba (SW Poland, Lower Silesia, Karkonosze Mts). In Proceedings of the International Symposium on Light Elements in Rock-forming Minerals, Nové Město na Moravě, Czech Republic, 20–25 June 2003; pp. 61–62.
25. Pieczka, A.; Gołębiowska, B. Cuprobismutite homologues in granitic pegmatites from Szklarska Poręba, Karkonosze Massif, Southwestern Poland. *Can. Mineral.* **2012**, *50*, 313–324. [[CrossRef](#)]
26. Pieczka, A. (AGH UST, Cracow, Poland); Gołębiowska, B. (AGH UST, Cracow, Poland). Personal communication, 2012.
27. Pouchou, I.L.; Pichoir, F. “PAP” (phi-rho-z) procedure for improved quantitative microanalysis. In *Microbeam Analysis*; Armstrong, I.T., Ed.; San Francisco Press: San Francisco, CA, USA, 1985; pp. 104–106.
28. Bruker. *SAINT*; Bruker AXS Inc.: Madison, WI, USA, 2007.
29. Sheldrick, G.M. *SADABS*; University of Göttingen: Göttingen, Germany, 1996.
30. Sheldrick, G.M. A short history of SHELX. *Acta Cryst.* **2008**, *A64*, 112–122. [[CrossRef](#)] [[PubMed](#)]
31. Cromer, D.T.; Waber, J.T. *International Tables for X-ray Crystallography, Volume IV*; The Kynoch Press: Birmingham, UK, 1974.
32. Ibers, J.A.; Hamilton, W.C. Dispersion corrections and crystal structure refinements. *Acta Cryst.* **1964**, *17*, 781–782. [[CrossRef](#)]
33. Creagh, D.C.; McAuley, W.J. X-ray dispersion corrections. In *International Tables for Crystallography, Volume C*; Kluwer Academic Publishers: Boston, MA, USA, 1992; pp. 219–222.
34. Creagh, D.C.; Hubbell, J.H. X-ray absorption (or attenuation) coefficients. In *International Tables for Crystallography, Volume C*; Kluwer Academic Publishers: Boston, MA, USA, 1992; pp. 200–206.
35. Aroyo, M.L.; Perez-Mato, J.M.; Capillas, C.; Kroumova, E.; Ivantchev, S.; Madariaga, G.; Kirov, A.; Wondratschek, H. Bilbao Crystallographic Server I: Databases and crystallographic computing programs. *Z. Krist.* **2006**, *221*, 15–27. [[CrossRef](#)]
36. Brese, N.E.; O’Keefe, M. Bond-valence parameters for solids. *Acta Cryst.* **1991**, *B47*, 192–197. [[CrossRef](#)]



© 2018 by the authors. Licensee MDPI, Basel, Switzerland. This article is an open access article distributed under the terms and conditions of the Creative Commons Attribution (CC BY) license (<http://creativecommons.org/licenses/by/4.0/>).